Effect of rotor Pole Shaping on Electromagnetic Performances of Consequent Pole Permanent Magnet Vernier Machine

Meysam Barghamadi[1], **Alireza Jaferian-Fini**[2], **Mohammad Ardebili**[3]

[1] Department of Electrical Engineering, K.N.Toosi University of Technology, Tehran, Iran; Meysam.Barghamadi@email.kntu.ac.ir
[2] Department of Electrical Engineering, K.N.Toosi University of Technology, Tehran, Iran; Alireza.Jaferian@email.kntu.ac.ir
[3] Department of Electrical Engineering, K.N.Toosi University of Technology, Tehran, Iran; ardebili@eetd.kntu.ac.ir

Abstract
Direct drive applications have become one of the most exciting research fields recently. Using the modulation effect (already known as the gearing effect), these kinds of machines can work at low speeds and have the low volume at the same time. Permanent magnet Vernier machine (PMVM) is one of these machines which have been the topic of papers during recent years. In order to reducing the quantity of PM material and hence cost, the Consequent pole permanent magnet (CPPM) machine has been proposed. This is why, in this paper, three different proposed structures of VPMs with surface-mounted permanent magnet Vernier (SPMV) machine, consequent pole with the same PM pole and iron pole shapes (CPPMV I) and consequent pole with the different PM pole and iron pole shapes (CPPMV II) are analyzed. Firstly, the structures and operating principles will be explained. Secondly, all three machines will be designed in the same condition but with different magnet volumes and finally, cogging torque, air-gap flux density harmonics and load torque of all machines will be studied. Under the same operation condition, the CPPMV II showed better performance compared with the other ones.
Keywords: Direct drive, Flux modulation, Consequent pole, Permanent magnet vernier machine (PMVM), Rotor pole shaping, Finite-element analysis (FEA).

Introduction

In recent years, direct drive machines have drawn increasing more attention for wind power generation, electric vehicles, marine propulsion and etc. [1]– [3]. In a direct drive system, by elimination of the gearbox, vibration and noise will be reduced and makes the drivetrain system much simpler and reliable. However, the high torque requirement at low speed makes the volume increase. Different permanent magnet machine topologies have been proposed to reduce the volume of direct drive machines such as transverse flux, axial flux and magnetically geared machines. However, these proposed machines have complex structure and multiple airgaps, which makes them difficult to manufacture. Meanwhile, due to having simple structure (Similar to conventional surface-mounted PM machines (SPM)) and high torque density at low speeds, permanent magnet Vernier (PMV) machine have been proposed for direct drive applications [4].

Vernier machines work based on the principle of flux modulation/magnetic gearing effect that makes them suitable candidate for direct drive topologies [5]. In recent years, many kinds of research have been conducted to improve Vernier machine performances such as improving power factor, torque density, reducing losses and cost. Based on these studies, different topologies have been proposed [6].

The price of rare-earth PM materials such as NdFeB is being increased continuously due to limited resources. Therefore, reduction of permanent magnet usage is necessary [7]. However, using very low-cost PM materials such as hard ferrites or reduced volume of rare-earth PM materials will make torque density diminish significantly. As a cost-effective solution, consequent pole (CP) PM machines, in which only alternate poles are equipped with a PM pole, have been suggested. These topologies are proven to achieve higher torque-to-PM volume ratios compared with their conventional SPM counterparts. Rotor pole shaping is an effective solution to reduce even-order harmonics due to unbalanced flux density distribution in CP machines. This reduction will be led to decrease torque ripple, cogging torque, vibration and noise [8].

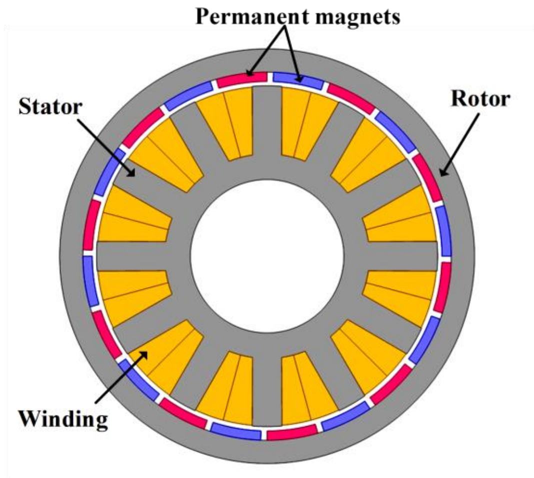

Figure 1. Example of an outer rotor SPMV machine with $Z=12$, $P_r=10$, $P_s=2$

In this article, first, the principles of operation Vernier machines are expressed. Then, to show effect of rotor pole shaping, three different topologies named surface-mounted permanent magnet Vernier (SPMV) machines, consequent pole with the same PM pole and iron pole shapes (CPPMV I) and consequent pole with the different PM pole and iron pole shapes (CPPMV II) are proposed. The electromagnetic performance of three types of machines is analyzed and compared by using finite-element analysis (FEA). Based on the analyzed results, the merits and demerits of them are discussed.

Machine Topology and Working Principle

A. Operation Principle

The 2D structure of a typical outer rotor PMV Machine with $Z=12$, $P_r=10$, $P_s=2$ is shown in "Figure 1". the operation principles of flux modulation machines in [9] are expressed. According to the general air-gap field modulation theory, The PMs generate the initial magnetomotive force (MMF) distribution. The modulators (salient stator poles) modulate the initial MMF distribution and produce working harmonics components $Z \pm P_r$ in air-gap flux density. The working harmonics of airgap flux density, attributed to the so-called magnetic gear effect, cause higher torque density than the conventional SPM machines. To maximize the utilization of these working harmonics components, the stator is wound the same as modulated pole pair. Therefore, the relationship between the number of rotor pole pairs, stator winding pole pairs and the stator slots should be satisfied as [10]:

$$P_r = Z \pm P_s \tag{1}$$

The Vernier machine is designed with slot/pole number combination given by $P_r=Z-P_s$, which generates higher torque than the one with $P_r=Z+P_s$ [11].

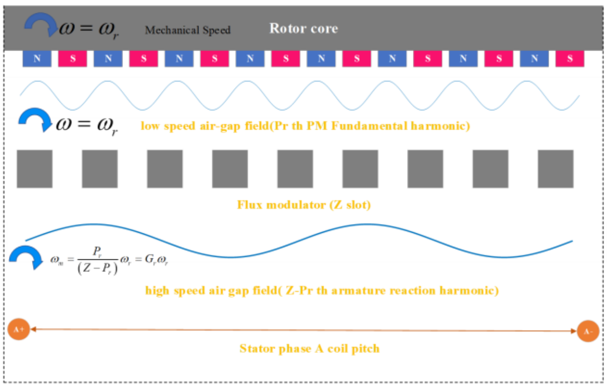

Figure 2. Schematic explanation of the magnetic gearing effect in vernier machines

"Figure 2" shows the number of pole pairs and the working magnetic fields speed. The low-speed direct drive rotor rotates at a mechanical speed of ω_r. The produced low-speed air-gap field is modulated by the Z stator teeth (air-gap permeance) and creates high speed air-gap field with fundamental and $(Z-P_r)$th order harmonics. These harmonics rotate at the angular speed of $[P_r/(Z-P_r)]\,\omega_r$. The ratio of the speed of the high-speed air gap field to that of the low-speed direct drive rotor is defined as the gear ratio (G_r) and is given by [12]:

$$G_r = \frac{(Z-P_s)}{P_s} = \frac{P_r}{P_s} \tag{2}$$

To achieve higher torque density, SPMV machines are generally designed with higher G_r. A high G_r is achieved by increasing P_r. However, A high number of rotor pole pairs increases PM flux leakage and consequently, causes poor power factor [10]. The no-load-induced EMF (E_{ph}) and average torque of the SPMV machines can be represented in terms of the air-gap flux density harmonics as [12], [13]:

$$E_{ph}^{rms} = \frac{D_g L_{stk} k_w N_{ph} \omega_r}{\sqrt{2}} \times \left(B_{P_r} + G_r B_{Z-P_r} - \frac{P_r}{(Z+P_r)} B_{Z+P_r} \right) \tag{3}$$

$$T_e = \frac{3}{\sqrt{2}} D_g L_{stk} N_{ph} k_w I_{ph} \times \left(B_{P_r} + G_r B_{Z-P_r} - \frac{P_r}{(Z+P_r)} B_{Z+P_r} \right) \tag{4}$$

With

$$\begin{cases} B_{P_r} = F_1 \Lambda_0 \\ B_{Z-P_r} = F_1 \Lambda_1 \\ B_{Z+P_r} = F_1 \Lambda_1 \\ F_1 = \dfrac{4\sin(\pi\alpha_p/2) B_r h_{Pm}}{\pi \mu_0 \mu_{r,pm}} \end{cases} \tag{5}$$

Where Λ_0 and Λ_1 are respectively the constant and fundamental components of air-gap permeance, which are calculated by conformal mapping [14].

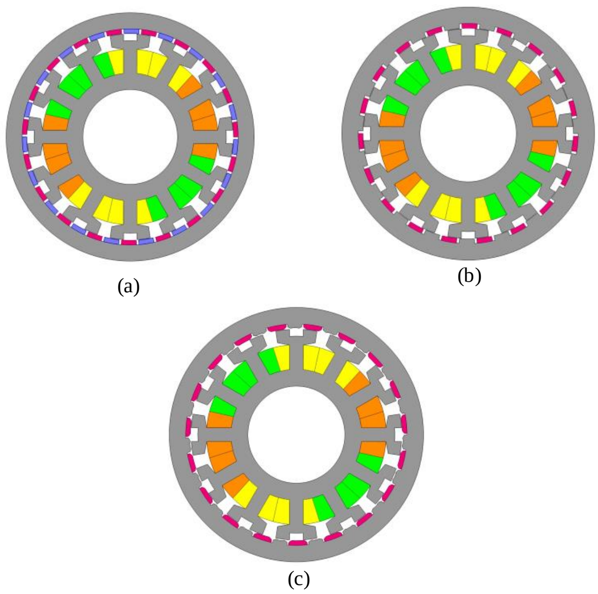

Figure 3. Machines topology. (a) SPMV. (b) CPPMV I. (c) CPPMV II.

B. Machines Topology

"Figure 3" shows the three types of Vernier machines with $Q=24$, $P_r=19$ and $P_s=5$. This slot/pole number combination is selected to offer a high winding factor and low cogging torque. All three Vernier machines have the same stator structure. To reduce end winding length, the fractional-slot concentrated winding (FSCW) with split-teeth structure has been used [15]. However, three types of machines adopt different PM arrangements in rotor configuration. A conventional SPMV rotor is illustrated in "Figure 3(a)". By direct replacement of the alternate PMs in SPMV machines with iron poles, the conventional CPPMV machine can be obtained in "Figure 3(b)". In CPPMV II, as shown in "Figure 3(c)", the PM pole and iron pole have specific shapes. The main parameters of the three machines are given in "Table 1".

Table 1. Main parameters of the three machines

Parameter	SPMV	CPPMV I	CPPMV II
ω_r	160(rpm)		
f	50(Hz)		
N_{ph}	360		
D_g	180(mm)		
L_{stk}	45(mm)		
g	0.5(mm)		
C_o	0.5(mm)		
B_r	1.2(T)		
h_{pm}	4(mm)		
α_p	0.85	0.85	0.93

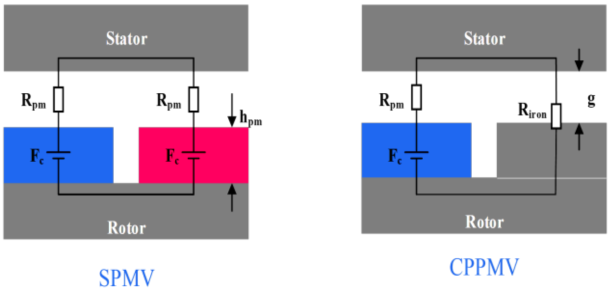

Figure 4. Magnetic circuit of SPMV and CPPMV machines for one pole pairs

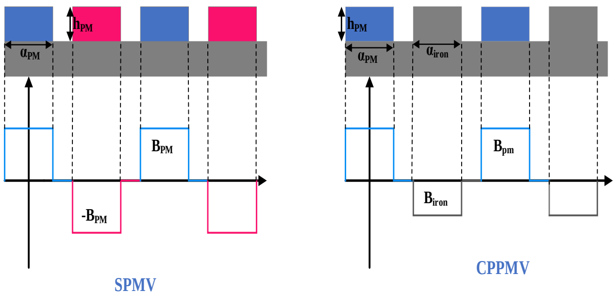

Figure 5. Flux density distribution of SPMV and CPPMV machines

Effect of rotor pole shaping in CPPMV Machine

"Figure 5" shows the flux density distribution of the SPMV and CPPMV machines. As it can be seen, one of the features of the CPPMV machine is the asymmetrical airgap magnetic field produced by the different nature of PM and iron poles. The asymmetrical air-gap magnetic field in the CPPMV machine gives rise to even-order harmonics in the air-gap field and can affect the electromagnetic performance of the machine. The magnetic circuit under one pole pair is demonstrated in "Figure 5" to show the principle of pole shaping. It was supposed that the relative permeabilities of the stator and rotor laminations in CPPMV machines are infinitive. The flux densities under PM pole and iron pole can be expressed as:

$$\begin{cases} B_{PM} = \dfrac{H_c L'_{mp} - F_s}{R_{PM} S_{p1}} \\ B_{iron} = \dfrac{\mu F_s}{g + h_{pm} - L'_{ip}} \end{cases} \tag{6}$$

With

$$\begin{cases} F_s = B_{iron} S_{p2} R_{iron} \\ R_{iron} = (g + h_{pm} - L'_{ip}) / \mu S_{p2} \end{cases} \tag{7}$$

Where H_c and F_s is the coercivity of magnet and magnetic potential in stator, respectively. L'_{mp} and L'_{ip} are the rotor profile functions which depend on the rotor position and can be expressed as by harmonic series:

$$\begin{cases} L'_{mp} = \sum_{a}^{\infty} [A_{msa} \sin(a\theta_r) + A_{mca} \cos(a\theta_r)] \\ L'_{ip} = \sum_{b}^{\infty} [A_{isb} \sin(b\theta_r) + A_{icb} \cos(b\theta_r)] \end{cases} \tag{8}$$

Equation (6) shows the relationship between the air-gap flux density and the rotor shape. So, reduction of L'_{mp} and L'_{ip} can increase flux density under the PM pole and iron pole. In this way, the average torque is improved. Moreover, the air-gap flux density distribution under the PM pole and iron pole is controlled by the magnetic potential of PMs and the air-gap magnetic reluctance, respectively. Therefore, it can be found that rotor pole shaping can affect electromagnetic performance of CPPMV machines and reduces even-order harmonics of air-gap flux density [8].

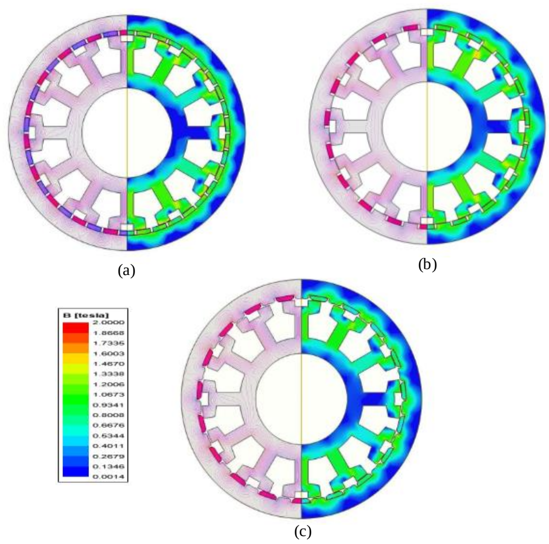

Figure 6. Flux density distribution and flux contours (a) SPMV. (b) CPPMV I. (c) CPPMV II.

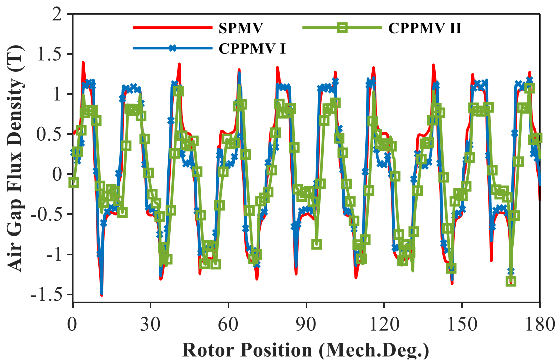

(a)

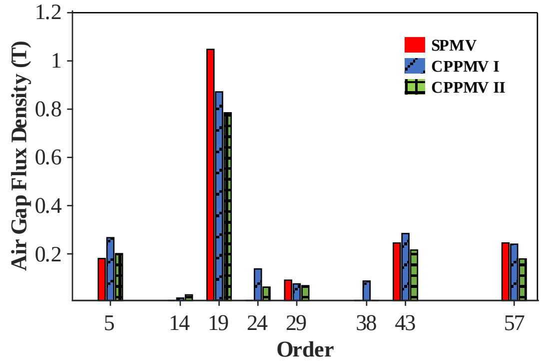

(b)

Figure 7. Air-gap flux density. (a) Waveforms. (b) Spectra.

Comparison of Electromagnetic Performances

A. Comparison of Air- Gap Flux Density

The no-load air-gap flux density waveforms and spectrum of harmonics of all three machines are shown in "Figure 7". It can be seen that the fundamental amplitude of air-gap flux density in the SPMV is the highest due to the larger PMs volume. The 5th, 29th and 43rd harmonics of air-gap flux density in the CPPMV II have the highest amplitude. However, the even-order harmonics of the CPPMV machines are the highest ones. The particular rotor pole shaping reduces the even-order harmonics in CPPMV II. As show in "Figure 6", the saturation levels of CPPMV II are the lowest due to decreasing harmonics amplitude.

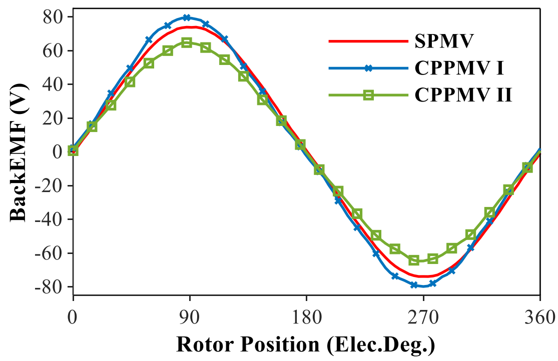

Figure 8. No-load Back-EMF waveform

B. No-Load Back EMF

"Figure 8" shows the comparison of no-load back EMF of all three machines. Due to having the highest order harmonics amplitude (5th, 43th) , the back EMF amplitude of CPPMV I is the more than the other machines. According to the slot/pole number combinations of and its effect on the elimination of even-order harmonics the winding flux linkage and as a result of back EMF, even-order harmonics are eliminated in the CPPMV machines [16]. Due to the decreasing harmonics amplitude, the back EMF waveform of the CPPMV II machine has better sinusoidal waveform than those of the other machines.

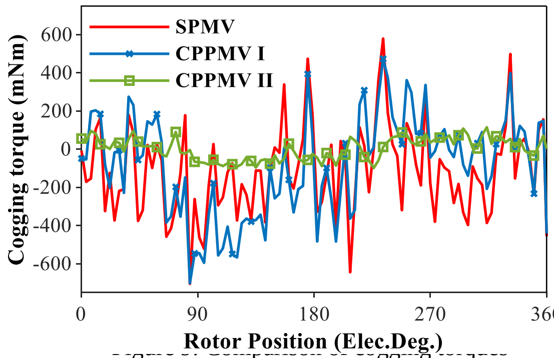

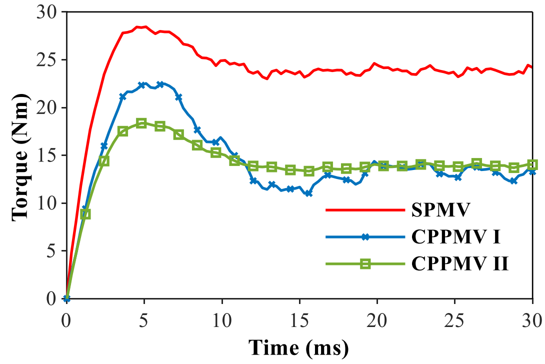

Figure 10. Comparison of torques

C. Comparison of Torque Performance

The pole arc-to-pole pitch ratio has a key effect on the cogging torque. By optimizing the pole arc coefficient, the cogging torque can be reduced [17]. "Figure 7" shows the comparison of cogging torque of three machines. The even order harmonics amplitude of CPPMV II are reduced. As a result, this machine has the lowest cogging torque. In "Figure 10", average torque and torque ripple of three machines are compared. It can be seen the CPPMV II has the lowest torque ripple and SPMV machine has the highest one. The comparison of torque parameters of three machines is given in "Table 2".

Table 3. Torque parameters analyzed machines

Parameter	SPMV	CPPMV I	CPPMV II
T_{av} (N.m)	23.82	13.09	13.82
η_{PM} (N.m/m^3)	269.43×10^3	296.13×10^3	275.2×10^3
T_r (%)	6	25	5.9
T_{cog} (%)	1.53	8.95	1.53

Conclusion

In this paper, three different topologies of the Vernier machine were investigated. These three machines were designed under the same condition but with different permanent magnet volumes. Airgap flux density, harmonic orders, no-load Back EMF, cogging torque and no-load torque were analyzed. The SPMV has a higher fundamental harmonic due to using all pole pairs. Therefore, it can be expected to have a higher average torque at steady-state conditions. Compared with the CPPMV machines, the negative point is higher peak-to-peak cogging torque. On the other side, the CPPMV machines have undeniable even-order harmonics in airgap flux density. Due to the presence of even harmonics, the CPPMV machines have a high torque ripple. The torque ripple and cogging torque of CPPMV I are improved with rotor shaping, which is presented as CPPMV II. Besides, the CPPMV II has more sinusoidal no-load EMF than those of the other machines and causes lower torque ripple at steady-state conditions. As a whole, for direct drive application, it can be said that the CPPMV II showed better performance from the view point of cogging torque, torque ripple and more sinusoidal waveform.

Nomenclatures

B_{Pr}	Fundamental air gap flux density
B_r	Remanent flux density
$B_{Z\pm Pr}$	Modulated air gap flux density
C_o	Slot opening
D_g	Air gap diameter
f	Frequency
F_1	Magnet fundamental component
g	Air gap length
G_r	Gear ratio
H_c	Coercivity of magnet
h_{pm}	PM thickness
I_{ph}	Phase current rms value
k_w	Winding factor
L_{stk}	Stack length
N_{ph}	Stator turns per phase
P_r	Rotor pole pairs
P_s	Stator pole pairs
Q	Modulator number
R_{iron}	Reluctances air gap under iron pole
R_{PM}	Reluctances air gap under PM pole
S_{p1}	Areas under the PM pole
S_{p2}	Areas under the iron pole
T_{av}	Average torque
T_{cog}	Cogging torque
T_r	Torque ripple
Z	Stator slot number
Λ_0	Fundamental air gap permeance function
Λ_1	DC air gap permeance function
α_p	Pole arc coefficient
η_{PM}	Torque to PM volume ratios
ω_r	Mechanical rotor speed

References

[1] H. Chen, Y. Zuo, K. T. Chau, W. Zhao, and C. H. T. Lee, “Modern electric machines and drives for wind power generation: A review of opportunities and challenges,” *IET Renewable Power Generation*, vol. 15, no. 9. John Wiley and Sons Inc, pp. 1864–1887, Jul. 01, 2021. doi: 10.1049/rpg2.12114.

[2] S. Madichetty, S. Mishra, and M. Basu, “New trends in electric motors and selection for electric vehicle propulsion systems,” *IET Electrical Systems in Transportation*, vol. 11, no. 3, pp. 186–199, Sep. 2021, doi: 10.1049/els2.12018.

[3] Z. Lu, G. Wu, M. Wang, Z. Luo, and J. Shang, “Design and Performance Analysis of a Staggered Vernier Generator for Wave Power Generation,” *J Mar Sci Eng*, vol. 10, no. 8, Aug. 2022, doi: 10.3390/jmse10081156.

[4] D. K. Kana Padinharu, G. J. Li, Z. Zhu, Z. Azar, R. Clark, and A. Thomas, “Effect of Airgap Length on Electromagnetic Performance of Permanent Magnet Vernier Machines with Different Power Ratings,” in *IEEE Transactions on Industry Applications*, 2022, vol. 58, no. 2, pp. 1920–1930. doi: 10.1109/TIA.2021.3135256.

[5] X. Zhu, C. H. T. Lee, C. C. Chan, L. Xu, and W. Zhao, “Overview of Flux-Modulation Machines Based on Flux-Modulation Principle: Topology, Theory, and Development Prospects,” *IEEE Transactions on Transportation Electrification*, vol. 6, no. 2, pp. 612–624, Jun. 2020, doi: 10.1109/TTE.2020.2981899.

[6] D. K. K. Padinharu *et al.*, “Permanent Magnet Vernier Machines for Direct-Drive Offshore Wind Power: Benefits and Challenges,” *IEEE Access*, vol. 10, pp. 20652–20668, 2022, doi: 10.1109/ACCESS.2022.3151968.

[7] B. Poudel, E. Amiri, P. Rastgoufard, and B. Mirafzal, “Toward Less Rare-Earth Permanent Magnet in Electric Machines: A Review,” *IEEE Transactions on Magnetics*, vol. 57, no. 9. Institute of Electrical and Electronics Engineers Inc., Sep. 01, 2021. doi: 10.1109/TMAG.2021.3095615.

[8] J. Qi *et al.*, “Effect of Pole Shaping on Torque Characteristics of Consequent Pole PM Machines,” *IEEE Trans Ind Appl*, vol. 58, no. 3, pp. 3511–3521, 2022, doi: 10.1109/TIA.2022.3156904.

[9] M. Cheng, P. Han, and W. Hua, “General Airgap Field Modulation Theory for Electrical Machines,” *IEEE Transactions on Industrial Electronics*, vol. 64, no. 8, pp. 6063–6074, Aug. 2017, doi: 10.1109/TIE.2017.2682792.

[10] D. K. K. Padinharu, G. J. Li, Z. Q. Zhu, R. Clark, Z. Azar, and A. Thomas, “Investigation of scaling effect on power factor of permanent magnet Vernier machines for wind power application,” *IET Electr Power Appl*, vol. 14, no. 11, pp. 2136–2145, Nov. 2020, doi: 10.1049/iet-epa.2020.0442.

[11] W. Liu and T. A. Lipo, “Analysis of Consequent Pole Spoke Type Vernier Permanent Magnet Machine with Alternating Flux Barrier Design,” *IEEE Trans Ind Appl*, vol. 54, no. 6, pp. 5918–5929, Nov. 2018, doi: 10.1109/TIA.2018.2856579.

[12] D. K. Kana Padinharu *et al.*, “Scaling Effect on Electromagnetic Performance of Surface-Mounted Permanent-Magnet Vernier Machine,”

IEEE Trans Magn, vol. 56, no. 5, May 2020, doi: 10.1109/TMAG.2020.2980500.

[13] L. Wu, R. Qu, D. Li, and Y. Gao, "Influence of Pole Ratio and Winding Pole Numbers on Performance and Optimal Design Parameters of Surface Permanent-Magnet Vernier Machines," *IEEE Trans Ind Appl*, vol. 51, no. 5, pp. 3707–3715, Sep. 2015, doi: 10.1109/TIA.2015.2426148.

[14] Z. Q. Zhu and D. Howe, "Instantaneous magnetic field distribution in brushless permanent magnet dc motors, Part III: Effect of stator slotting," *IEEE Trans Magn*, vol. 29, no. 1, pp. 143–151, 1993, doi: 10.1109/20.195559.

[15] L. Xu, G. Liu, W. Zhao, X. Yang, and R. Cheng, "Hybrid Stator Design of Fault-Tolerant Permanent-Magnet Vernier Machines for Direct-Drive Applications," *IEEE Transactions on Industrial Electronics*, vol. 64, no. 1, pp. 179–190, Jan. 2017, doi: 10.1109/TIE.2016.2610399.

[16] J. Qi *et al.*, "Influence of slot/pole number combinations and pole shaping on electromagnetic performance of permanent magnet machines with unbalanced north and south poles," *IET Electr Power Appl*, 2023, doi: 10.1049/elp2.12293.

[17] H. Zhou, W. Tao, C. Zhou, Y. Mao, G. J. Li, and G. Liu, "Consequent pole permanent magnet vernier machine with asymmetric air-gap field distribution," *IEEE Access*, vol. 7, pp. 109340–109348, 2019, doi: 10.1109/ACCESS.2019.2933657.